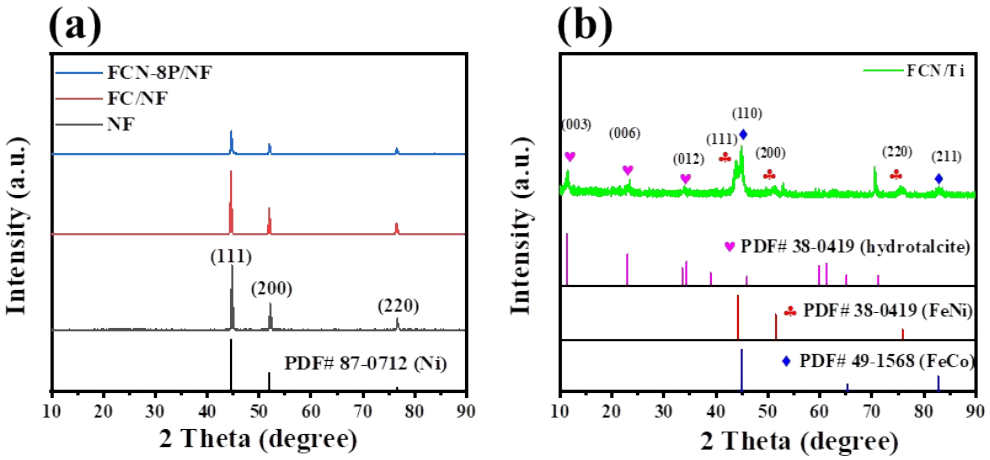

Fig. S1 (a) XRD patterns of FCN-8P/NF, FC/NF, and NF. (b) XRD pattern of FCN/Ti.

Note.1: **Fig. S1**(b) shows the XRD pattern of FCN on Ti foil, and exhibits apparent peaks at 11.43°, 22.98°, and 34.44° corresponding to (003), (006), and (012) planes of hydrotalcite (PDF# 40-0215). Peaks at 44.27°, 51.55°, and 75.87° belong to (111), (200), and (220) planes of FeNi (PDF# 38-0419). Other peaks appearing in 44.88°, 65.31°, and 82.75° can be indexed to (110), (200), and (211) planes of FeCo (PDF# 49-1568). The above results mean that the phase of FCN is crystalline FeCoNi alloy/FeCoNi-LTHs.

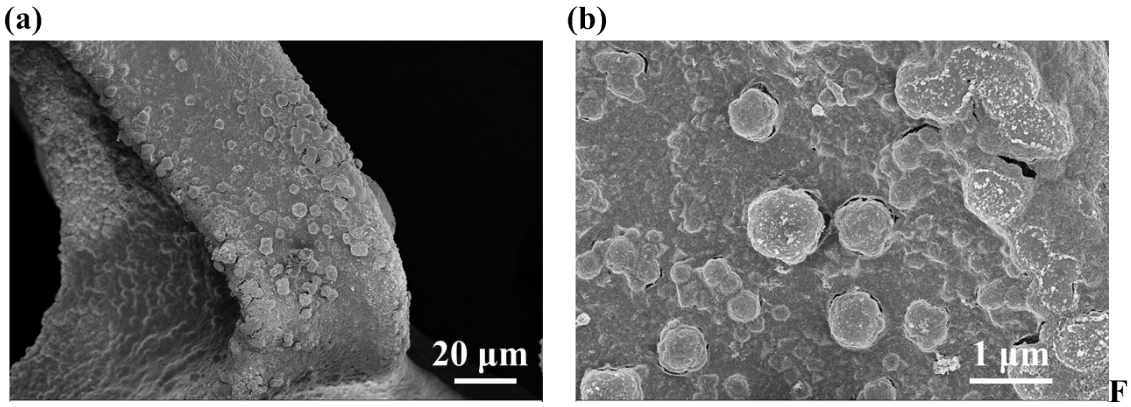

Fig. S2 (a)-(b) SEM images of FC on NF.

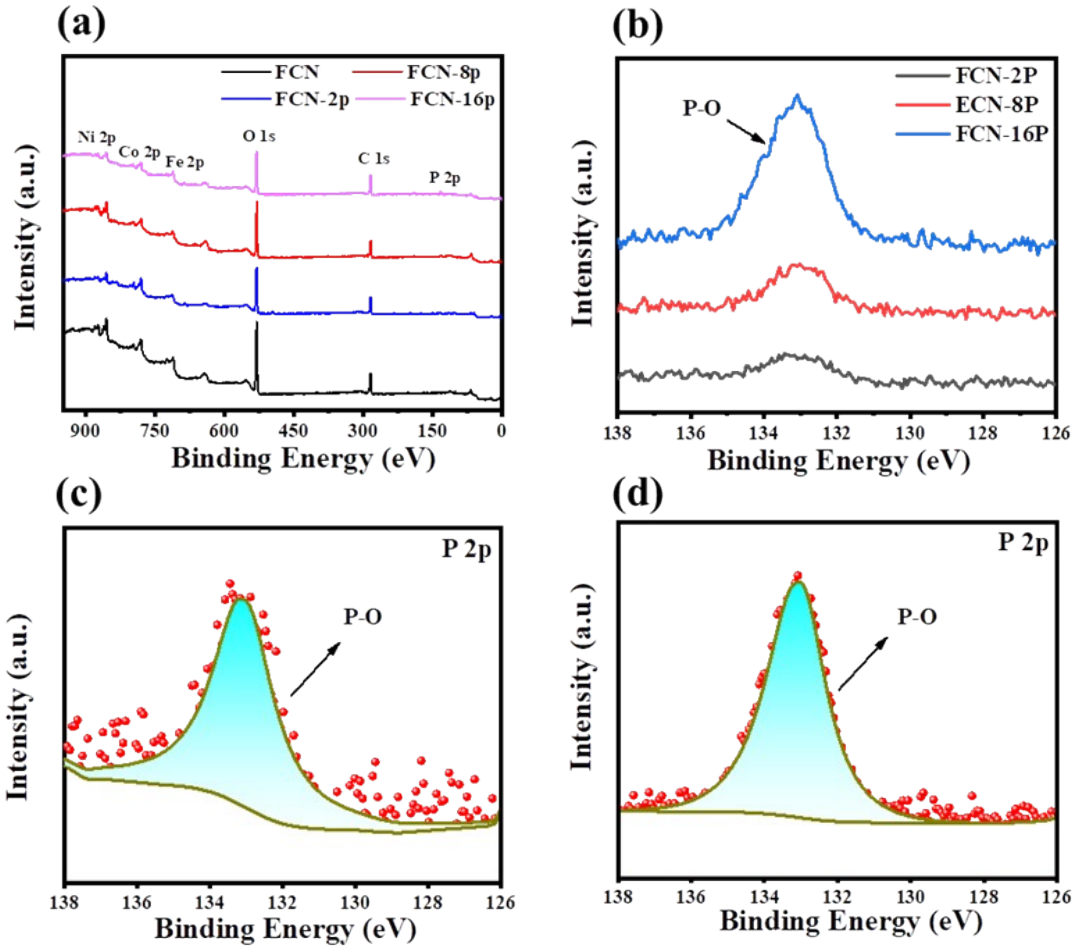

Fig. S3 (a) XPS full spectra of FCN, FCN-2P, FCN-8P and FCN-16P. (b) P 2p of FCN-2p, FCN-8P, FCN-16P. (c) High-resolution XPS spectra of P 2p in FCN-2p. (d) High-resolution XPS spectra of P 2p in FCN-16p.

Table S1 The HER overpotential value of different electrodeposited samples to attain the current densities of 10 mA cm^{-2} and 100 mA cm^{-2} respectively.

Electrocatalysts	η@10 mA cm^{-2}	η@100 mA cm^{-2}
FC	**179 mV**	**281 mV**
FCN	**126 mV**	**248 mV**
FCN-2P	**122 mV**	**221 mV**
FCN-4p	**103 mV**	**215 mV**
FCN-8P	**77 mV**	**201 mV**
FCN-12p	**96 mV**	**212 mV**
FCN-16p	**102 mV**	**217 mV**

Amorphous phosphate can promote the adsorption and dissociation of water molecules and improve the hydrophilicity of materials. However, its adsorption and desorption ability for protons is not as good as that of crystalline FeCo alloy. To achieve optimal activity for FeCo alloy/FeCoNi-Pi, it's important to adjust the appropriate amorphous phosphate content. With the increase of $NaH_2PO_2.H_2O$ dosage, the amorphous phosphate content in the crystalline/amorphousFeCoalloy/FeCoNi-Pi also increases during sample preparation. The sample can be given an optimal phosphate content with 8P.

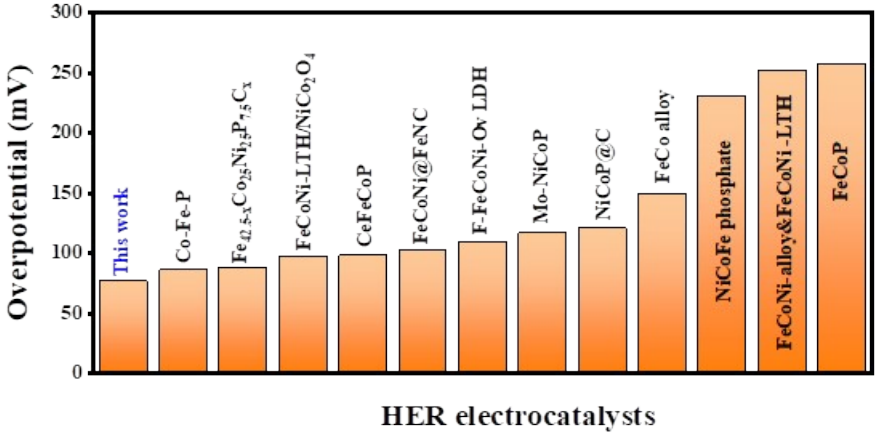

Fig. S4 Comparison of HER performance at 10 mA cm^{-2} with recently reported FeCoNi-based electrocatalysts. References cited in Fig. S : Co-Fe-P[S1], $Fe_{42.5-x}Co_{25}Ni_{25}P_{7.5}C_x$[S2], FeCoNi-LTH/$NiCo_2O_4$[S3], CeFeCoP[S4], FeCoNi@FeNC[S5], F-FeCoNi-Ov LDH[S6], Mo-NiCoP[S7], NiCoP@C[S8], FeCo alloy[S9], NiCoFe phosphate[S10], FeCoNi-alloy&FeCoNi – LTH[S11], and FeCoP [S12].

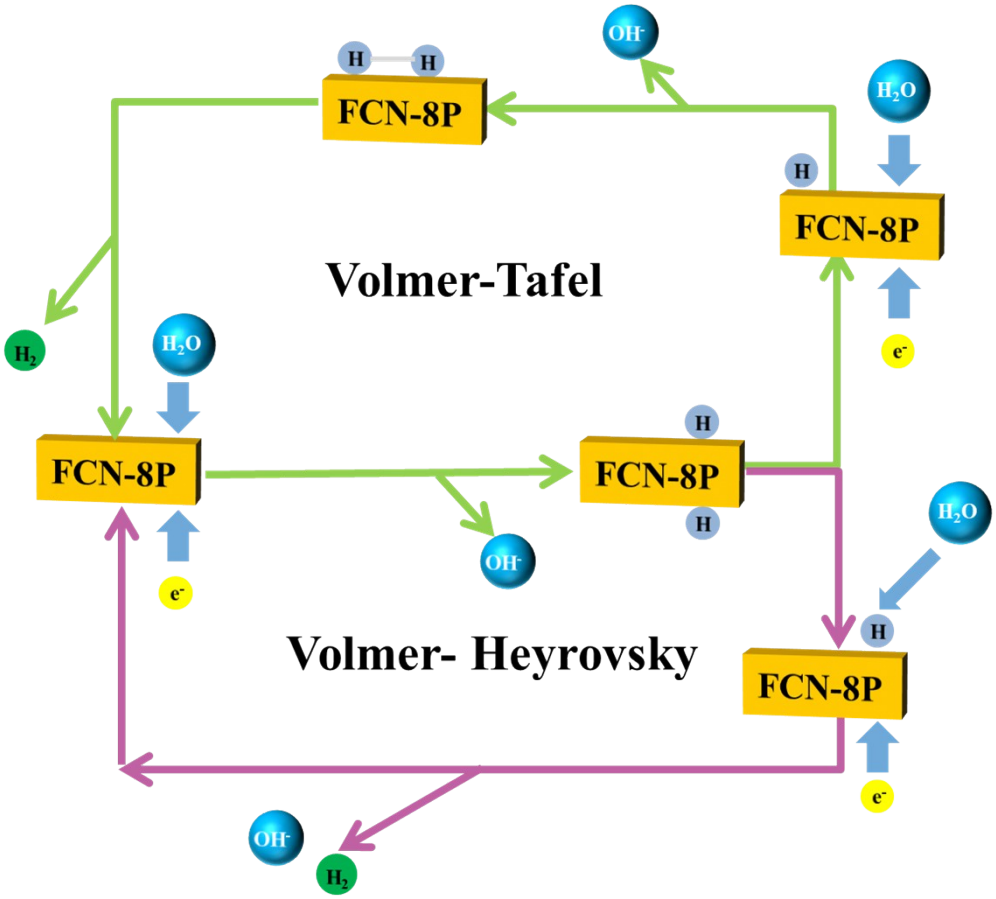

Fig. S5 The HER mechanism of FCN-8P.

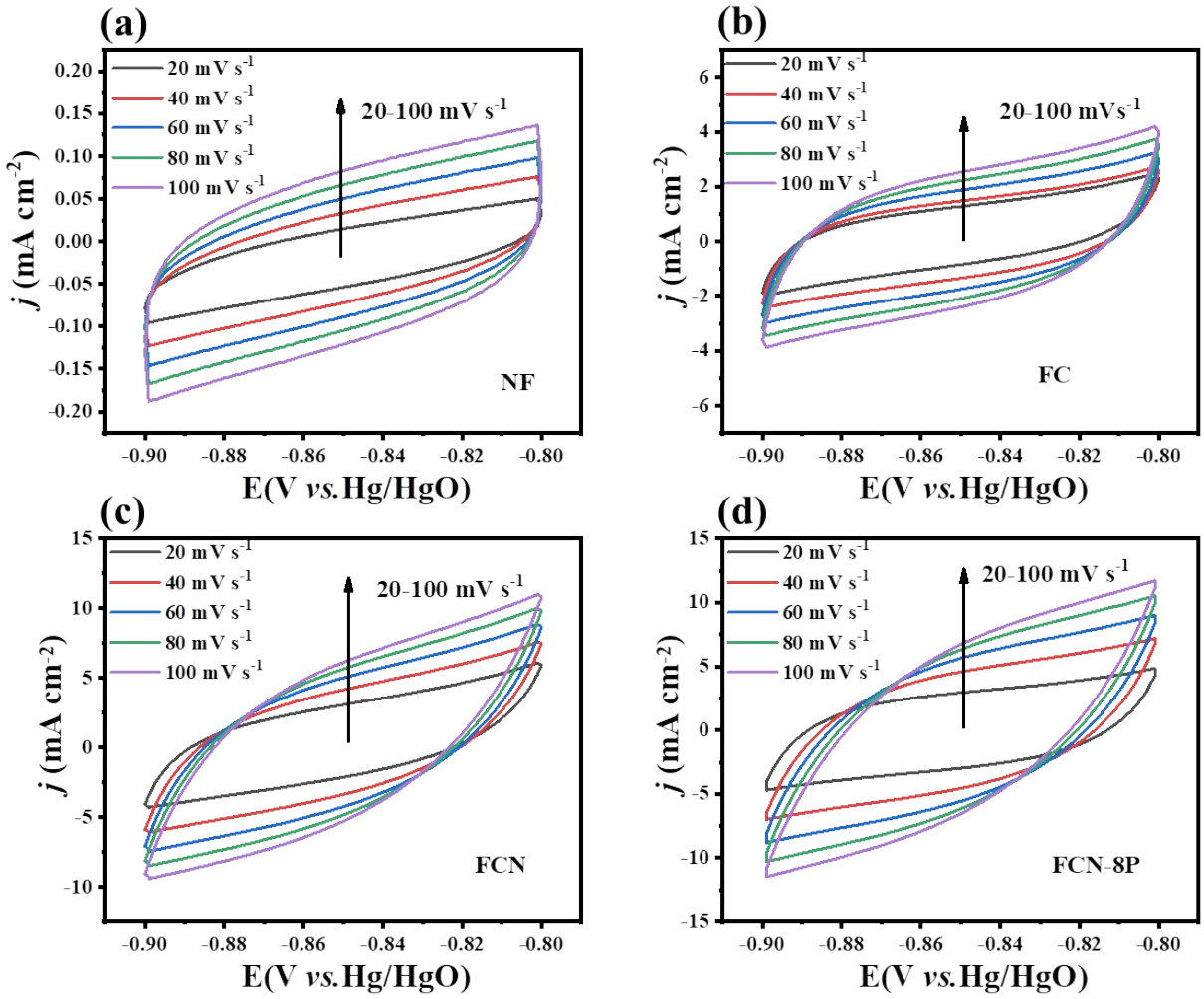

Fig. S6 Electrochemical active surface area analysis by the CV scans in a non-Faradaic potential range of as-prepared electrodes for HER (a) NF, (b) FC, (c) FCN, (d) FCN-8P.

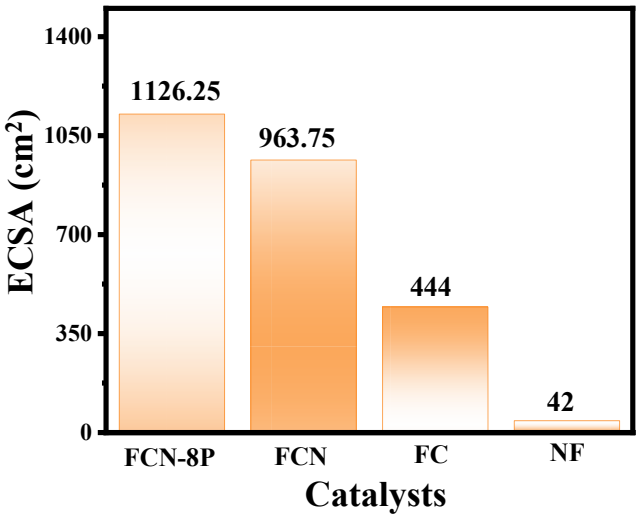

Fig. S7 The ECSA values of FCN-8P, FCN, FC, and NF for HER.

Table S2 The Rct Value of different electrocatalysts for HER

Electrocatalysts	Rct
FC	**1.067 Ω**
FCN	**0.611 Ω**
FCN-8P	**0.392 Ω**

Table S3 The OER overpotential value of different electrodeposited samples to attain the current densities of 10 mA cm^{-2} and 100 mA cm^{-2} respectively.

Electrocatalysts	η@10 mA cm^{-2}	η@100 mA cm^{-2}
FC	**267 mV**	**321 mV**
FCN	**250 mV**	**302 mV**
FCN-2P	**248 mV**	**304 mV**
FCN-4p	**246mV**	**297mV**
FCN-8P	**233 mV**	**284 mV**
FCN-12p	**237mV**	**287mV**
FCN-16p	**236 mV**	**289 mV**

To achieve optimal activity for FeCo alloy/FeCoNi-Pi, it's important to adjust the appropriate amorphous phosphate content. With the increase of $NaH_2PO_2.H_2O$ dosage, the amorphous phosphate content in the crystalline/amorphousFeCoalloy/FeCoNi-Pi also increases during sample preparation. The sample can be given an optimal phosphate content with 8P.

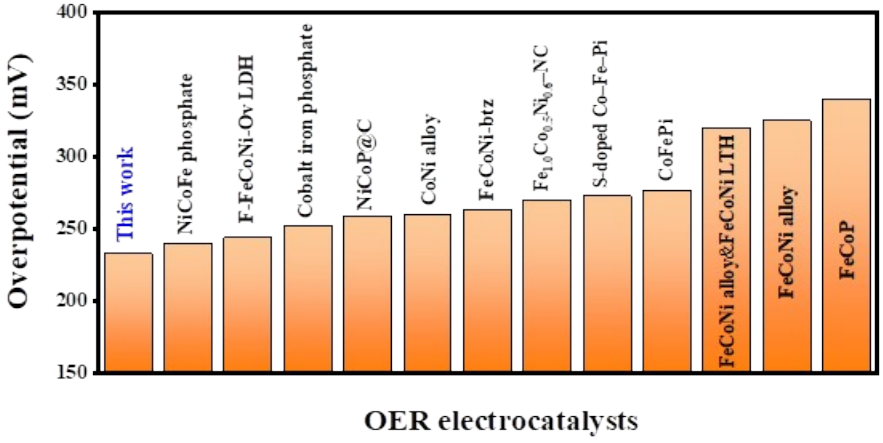

Fig. S8 Comparison of OER performance at 10 mA cm^{-2} with recently reported FeCoNi-based electrocatalysts. References cited in Fig. S : NiCoFe phosphate[S10], F-FeCoNi-Ov LDH[S6], Cobalt iron phosphate[S13], NiCoP@C[S8], CoNi alloy[S14], FeCoNi-btz[S15], $Fe_{1.0}Co_{0.5}Ni_{0.6}$–NC[S16], S-doped Co–Fe–Pi[S17], CoFePi[S18], FeCoNi-alloy&FeCoNi – LTH[S11], FeCoNi alloy[S9], and FeCoP[S12].

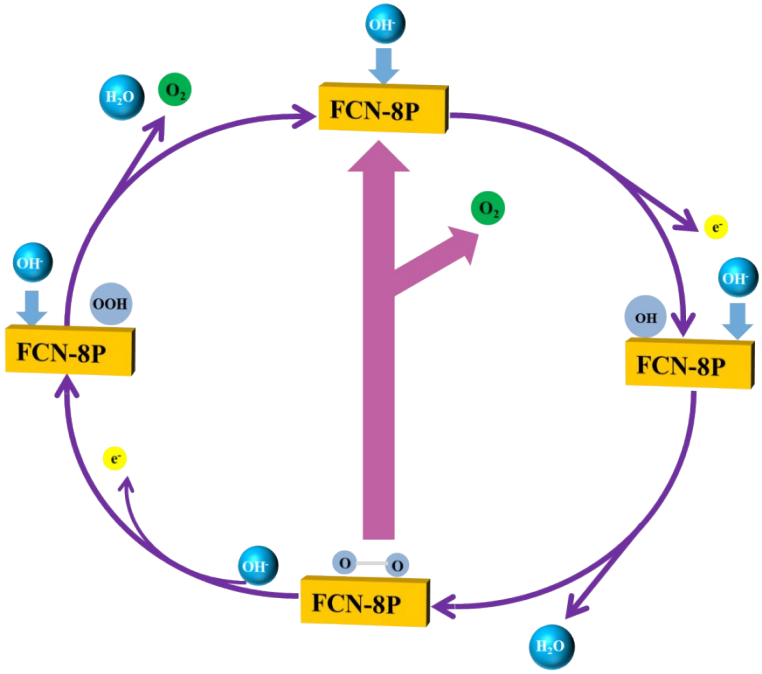

Fig. S9 the OER mechanism of FCN-8P.

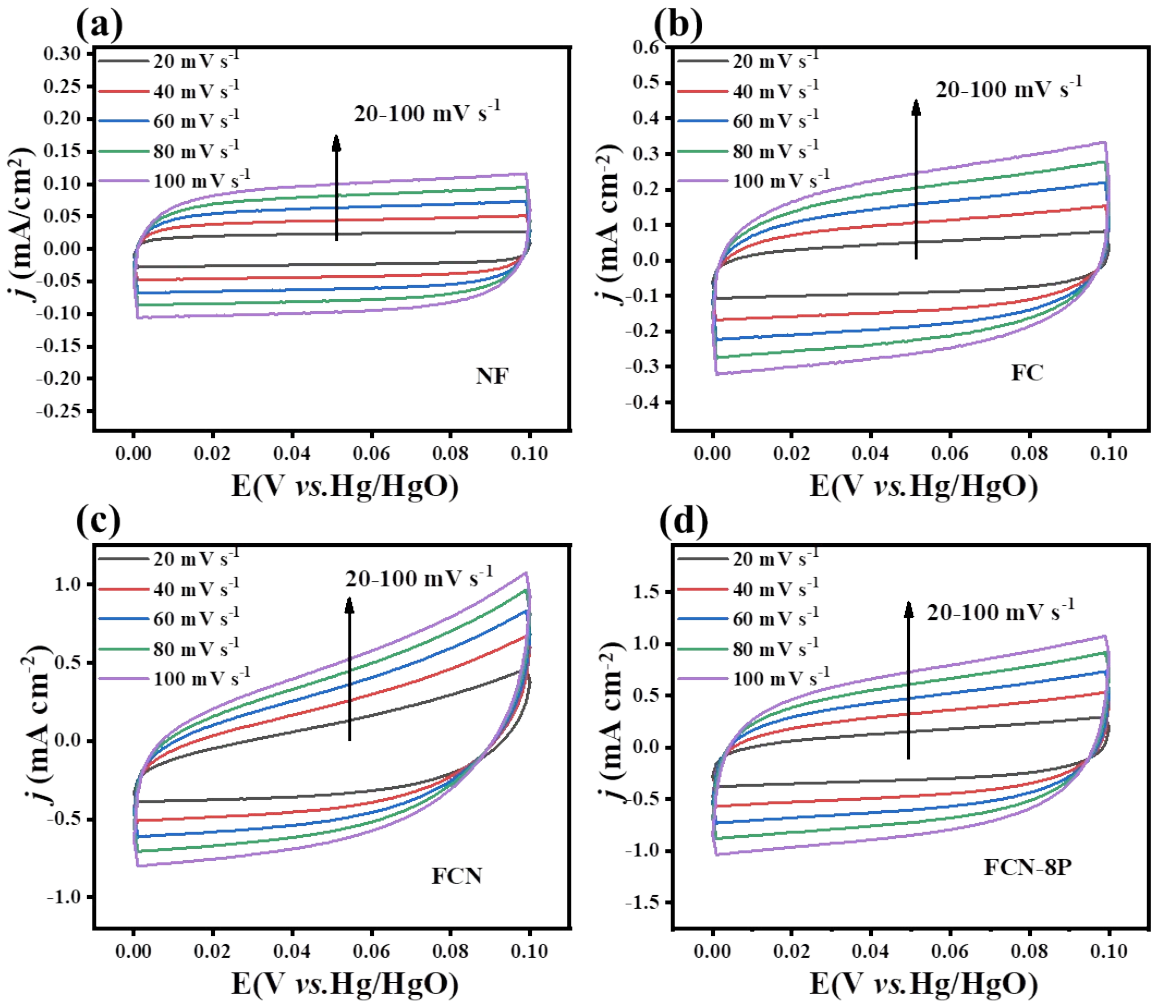

Fig. S10 Electrochemical active surface area analysis by the CV scans in a non-Faradaic potential range of as-prepared electrodes for OER (a) NF, (b) FC, (c) FCN, (d) FCN-8P.

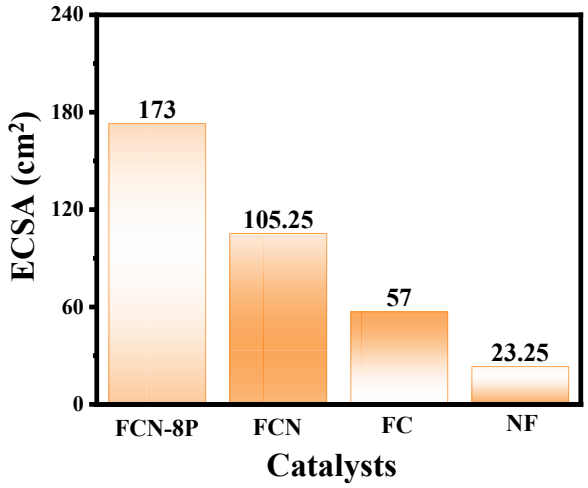

Fig. S11 The ECSA values of FCN-8P, FCN, FC, and NF for OER.

Table S4 The Rct Value of different electrocatalysts for OER

Electrocatalysts	Rct
FC	**0.540 Ω**
FCN	**0.359 Ω**
FCN-8P	**0.297 Ω**

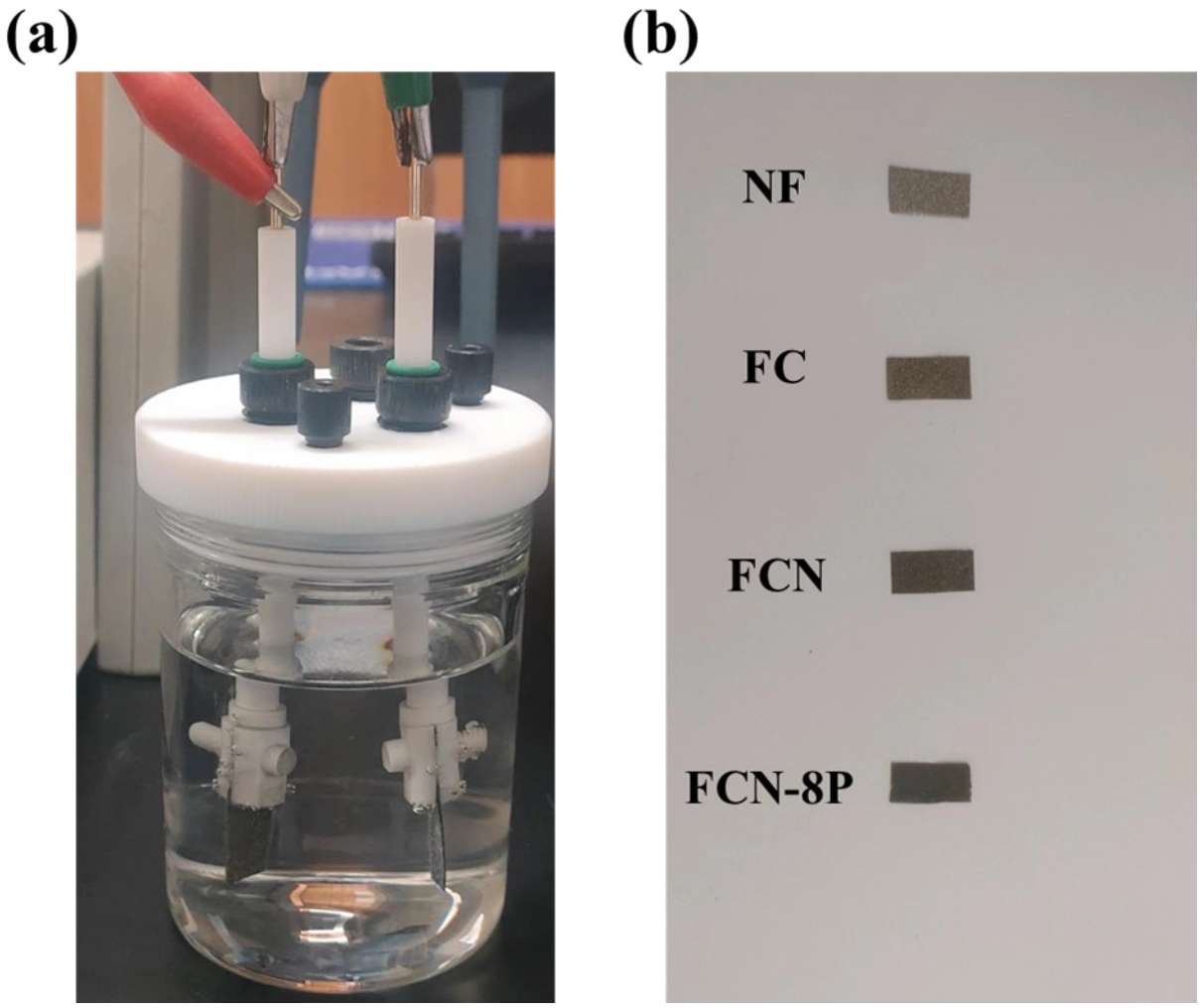

Fig. S12 (a) Optical picture of the water-splitting device. (b) Optical pictures of the electrodeposition samples.

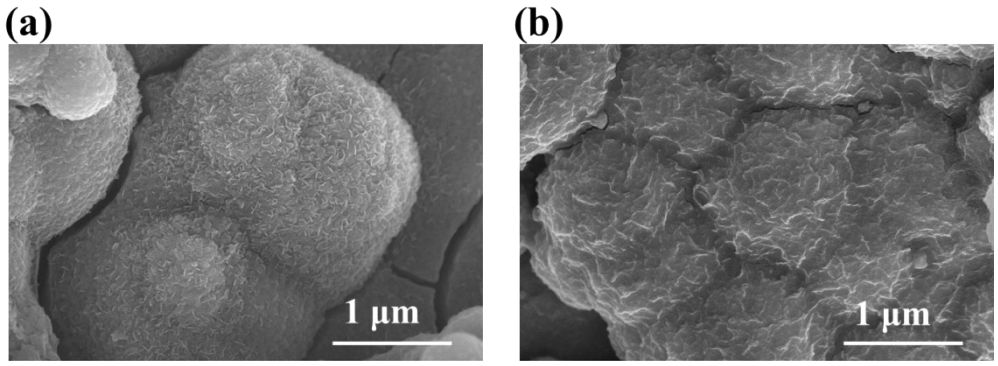

Fig. S13 (a) SEM image of FCN-8P electrocatalyst after long-term OER process. **(b)** SEM image of FCN-8P electrocatalyst after long-term HER process.

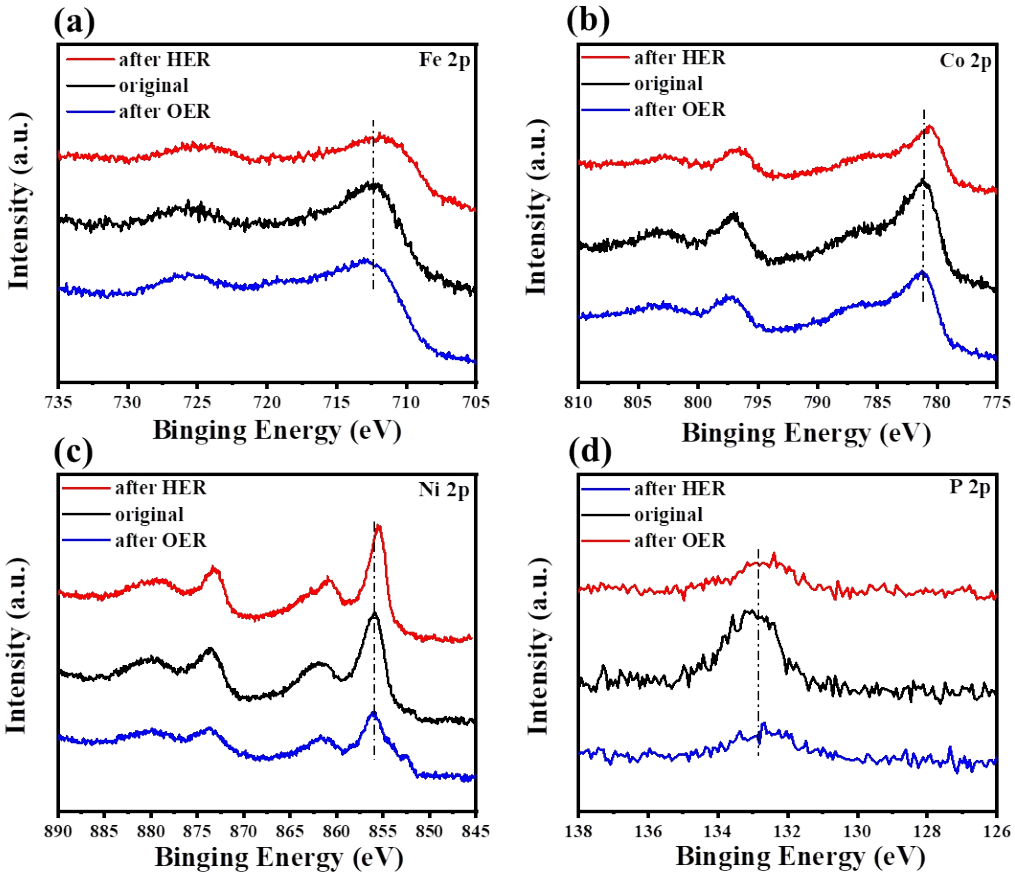

Fig. S14 High-resolution XPS spectra of (a) Fe 2p, (b) Co 2P, (c) Ni 2p, and (d) P 2p in FCN-8P electrode after long-term stability test.

Reference

[S1]. J. Chen, J. Liu, J.-Q. Xie, H. Ye, X.-Z. Fu, R. Sun and C.-P. Wong, Co-Fe-P nanotubes electrocatalysts derived from metal-organic frameworks for efficient hydrogen evolution reaction under wide pH range, *Nano Energy*, 2019, **56**, 225-233.

[S2]. Y. Lu, S. Xu, L. Zhang, Q. Hu, J. Song, F. Zhang and B. Zhang, The characteristics of excellent electrocatalytic hydrogen evolution for FeCoNi based high entropy alloys, *Sustainable Mater.Technol.*, 2022, **33**, e00455.

[S3]. Y. Liu, Y. Bai, Y. Han, Z. Yu, S. Zhang, G. Wang, J. Wei, Q. Wu and K. Sun, Self-Supported Hierarchical FeCoNi-LTH/NiCo2O4/CC Electrodes with Enhanced Bifunctional Performance for Efficient Overall Water Splitting, *ACS Appl. Mater. Interfaces*, 2017, **9**, 36917-36926.

[S4]. L. Shen, S. Tang, L. Yu, Q. Huang, T. Zhou, S. Yang, H. Yu, H. Xiong, M. Xu, X. Zhong and L. Zhang, Efficient ternary CeFeCoP bifunctional electrocatalyst for overall water splitting, *J. Solid State Chem.*, 2022, **314**, 123434.

[S5]. Q. Zhang, R. F. Webster, S. Cheong, R. D. Tilley, X. Lu and R. Amal, Ultrathin Fe-N-C Nanosheets Coordinated Fe-Doped CoNi Alloy Nanoparticles for Electrochemical Water Splitting, *Particle & Particle Systems Characterization*, 2019, **36**, 1800252.

[S6]. Z. Zhai, W. Yan and J. Zhang, Layered FeCoNi double hydroxides with tailored surface electronic configurations induced by oxygen and unsaturated metal vacancies for boosting the overall water splitting process, *Nanoscale*, 2022, **14**, 4156-4169.

[S7]. C. Sun, Y. He, N. S. Alharbi, S. Yang and C. Chen, Three-dimensional ordered macroporous molybdenum doped NiCoP honeycomb electrode for two-step water electrolysis, *J. Colloid Interface Sci.*, 2023, **642**, 13-22.

[S8]. X. Liu, G. Xu, H. Ding, L. Zhang and T. Huang, NiCoP nanoparticles embedded in coal-based carbon nanofibers as self-supporting bifunctional electrocatalyst toward water splitting, *Int. J. Hydrogen Energy*, 2023, **48**, 35064-35074.

[S9]. Y. Yang, Z. Lin, S. Gao, J. Su, Z. Lun, G. Xia, J. Chen, R. Zhang and Q. Chen, Tuning Electronic Structures of Nonprecious Ternary Alloys Encapsulated in Graphene Layers for Optimizing Overall Water Splitting Activity, *ACS Catal.*, 2017, **7**, 469-479.

[S10]. M. A. Z. G. Sial, H. Lin and X. Wang, Microporous 2D NiCoFe phosphate nanosheets supported on Ni foam for efficient overall water splitting in alkaline media, *Nanoscale*, 2018, **10**, 12975-12980.

[S11]. Q. Liu, Z. Yan, J. Gao and E. Wang, Surface-Oxidized Iron–Cobalt–Nickel Alloy with Continuous Variable Composition for Hydrogen and Oxygen Evolution Reaction, *ACS Sustainable Chem. Eng.*, 2022, **10**, 14926-14934.

[S12]. M. Streckova, O. Petrus, A. Guboova, R. Orinakova, V. Girman, C. Bera, M. Batkova, M. Balaz, J. Shepa and J. Dusza, Nanoarchitectonics of binary transition metal phosphides embedded in carbon fibers as a bifunctional electrocatalysts for electrolytic water splitting, *J. Alloys Compd.*, 2022, **923**, 166472.

[S13]. S. A. Khalate, S. A. Kadam, Y.-R. Ma, S. B. Kulkarni, V. G. Parale and U. M. Patil, Binder free cobalt iron phosphate thin films as efficient electrocatalysts for

overall water splitting, *J. Colloid Interface Sci.*, 2022, **613**, 720-732.

[S14]. M. A. Ehsan, A. Khan and A. S. Hakeem, Binary CoNi and Ternary FeCoNi Alloy Thin Films as High-Performance and Stable Electrocatalysts for Oxygen Evolution Reaction, *ACS Appl. Energy Mater.*, 2023, **6**, 9556-9567.

[S15]. S. Li, Z. Wang, T. Wang, Y. Yang, Y. Xiao, Y. Tian, H. Zhu, X. Jing and G. Zhu, Preparation of Trimetallic-Organic Framework Film Electrodes via Secondary Growth for Efficient Oxygen Evolution Reaction, *Chemistry – A European Journal*, 2023, **29**, e202301129.

[S16]. M. Khalid, A. M. B. Honorato, G. Tremiliosi Filho and H. Varela, Trifunctional catalytic activities of trimetallic FeCoNi alloy nanoparticles embedded in a carbon shell for efficient overall water splitting, *J. Mater. Chem. A*, 2020, **8**, 9021-9031.

[S17]. Q. Yue, T. Gao, Y. Wu, H. Yuan and D. Xiao, S-doped Co-Fe-Pi nanosheets as highly efficient oxygen evolution electrocatalysts in alkaline media, *Electrochim. Acta*, 2020, **362**, 137123.

[S18]. Y. Zhou and H. C. Zeng, 3D Networks of CoFePi with Hierarchical Porosity for Effective OER Electrocatalysis, *Small*, 2018, **14**, 1704403.